# Supplementary material

# for

# Investigating the D" reflector beneath the Indian Ocean with source arrays

Christine Thomas[1,2*], Björn Heyn[3], Lena Sophie Tölle[1], Rûna van Tent[1]

[1] Institute of Geophysics, University of Münster, Germany
[2] Geological Survey of Denmark and Greenland, Copenhagen, Denmark
[3] Centre for Planetary Habitability (PHAB), Department of Geosciences, University of Oslo, Norway
[*]Corresponding author: cthom_01@uni-muenster.de

**Author ORCIDs**
C. Thomas: 0000-0002-7845-5385
B.H. Heyn: 0000-0003-1685-6674L.S. Tölle: 0009-0009-4060-0979
R. van Tent: 0009-0005-7274-8370

This supplementary material contains information on source normalisation methods, tables with station locations as well as earthquake locations taken from National Earthquake Information Centre (NEIC), used for either the Indian Ocean (IO or MSEY) or stations in Antarctica (MAW, DRV, CASY). Additionally, the two events used for receiver arrays (see Figure S8) are given in Table S3.

Supplementary figures show seismic traces (Z-components) for source arrays for stations FOMA, DRV, AIS and PAF (Figure S1), traces and different source normalisation methods for PAF (Figure S2). Figure S3 shows a vespagram stack with P as reference phase compared with PcP as reference phase. An explanation of picking using the migration images is shown in Figure S4. Amplitude-depth profiles and migration images for stations CRZF and PAF are given in Figure S5 and for MAW, CASY and MSEY in Figure S6. A test for a 3D model without reflector is shown in Figure S9, this test shows that finite frequency effects cannot generate the signals interpreted in the study. For further verification of our results, we show two events recorded at receiver arrays in Madagascar and Tanzania that show D" reflections in P and S-waves (Figure S8), we also included results from two events recorded in Australia, whose reflection points are also in the north of our study region and further east as shown in Figures 9 and S9. Figure S9 shows the results on the vote map for P-wave tomographic models (similar to Figure 9) for lower than average seismic velocities.

**Details for source normalisation methods:**

SD is the most commonly employed method, where each recorded trace is deconvolved by its corresponding P-wavelet (same applies for S-waves), and this method has been used in previous source- and double-array studies (e.g., Krüger et al., 1996; Thomas et al., 2002; Lay and Garnero, 2011). In an ideal case, this results in a trace with Gaussian-shaped spikes that correspond to recorded P-wave signals (e.g., P, PdP, PcP), thus making the signals from different earthquakes coherent. While this method is not very sensitive to the P-wavelet time window length, it is strongly affected by the presence of noise or other signals that may overlap with the P-wavelet. As a consequence, it is less reliable for noisy data, such as the

recordings from stations located on small oceanic islands (Beucler et al., 2015), but potentially also for land stations (Anthony et al., 2022).

Since coherent phases are expected to have the same phase (or a phase shift by $\pm \frac{\pi}{2}$ for signals with reversed polarity), while noise can be assumed to have a random phase (Shearer, 2009), it might be helpful to include phase information in the deconvolution process to discriminate between signal and noise. Therefore, we also tried applying a Hilbert transform to the recorded P-wavelet (but not to the trace itself) before carrying out the deconvolution as described above. The HIL method applies a phase shift of $\frac{\pi}{2}$ to the Fourier coefficients of the wavelet, but it does not affect the amplitude spectrum nor the relative polarities of the recorded signals (e.g., Dahlen and Tromp, 1998; Shearer, 2009). While this method should produce better results for noisy data that have clearly visible P-waveforms, it is sensitive to the length of a deconvolution time window, especially if that time window does not contain the entire P-wavelet. As a consequence, this method works best for data with very clear P-wavelets or slightly longer deconvolution windows.

In addition to the two deconvolution methods described above, we also tried cross-correlating the recorded P-wavelet with its respective seismogram (Schimmel and Paulsen, 1997). The CORR method measures the similarity between the input wavelet and the respective part of the trace; therefore, it only depends on waveform coherency within a single seismogram. Although mathematically similar to the SD approach, CORR leads to broader, symmetric waveforms. It also avoids deconvolution sidelobes (Oldenburg, 1981). The CORR method is less sensitive to noise in the P-wavelet than the SD technique, but the resulting wide waveforms can mask or merge signals that arrive shortly after one other.

The final method we tried, but which was unsuccessful for our purposes, is the iterative ID approach (Ligorria and Ammon, 1999), is typically applied in receiver function analyses. This method is a combination of correlation and deconvolution, which iteratively creates a trace of spikes that correspond to specific signals. However, due to the sharp spike waveform (even after applying a Gaussian filter to broaden the signals), any small deviations in relative travel-times between phases (e.g., due to errors in source depths) causes the respective signal to disappear in the stack. As a result, this method is, at the moment, not well suited for vespagram stacks, and therefore is only of limited use for source-array stacking of teleseismic waves. We just mentioned it here for completeness.

**References:**


Anthony, R. E., A. T. Ringler, and D. C. Wilson (2022). Seismic Background Noise Levels across the Continental United States from USArray Transportable Array: The Influence of Geology and Geography*, Bulletin of the Seismological Society of America* 112, 646–668, doi.org/10.1785/0120210176

Beucler, É., Mocquet, A., Schimmel, M., Chevrot, S., Quillard, O., Vergne, J., and Sylvander M. (2015), Observation of deep water microseisms in the North Atlantic Ocean using tide modulations, *Geophysical Research Letters,* 42, 316–322, doi.org/10.1002/2014GL062347

Dahlen, F.A., and Tromp, J., (1998). *Theoretical Global Seismology,* Princeton University Press, pp. 552-524.

Ebinger. C., (2013). *Magadi-Natron Magmatic Rifting Studies* [Data set]. International Federation of Digital Seismograph Networks. https://doi.org/10.7914/SN/XJ_2013

Krüger, F., Scherbaum, F., Weber, M., and Schlittenhardt, J. (1996). Analysis of asymmetric multipathing with a generalization of the double-beam method. *Bulletin of the Seismological Society of America*, 86(3), 737-749, doi.org/10.1785/BSSA0860030737.

Lay T., and Garnero E.J., (2011). Deep mantle seismic modeling and imaging. *Annual Review of Earth and Planetary Sciences*, 39(39), 91–123. doi.org/10.1146/annurev-earth-040610-133354.

Leng, K., Nissen-Meyer, T., Van Driel, M., Hosseini, K., Al.Attar, D., (2019). AxiSEM3D: broad-band seismic wavefields in 3-D global earth models with undulating discontinuities. *Geophys. J. Int.,* 217, 2125-2146, doi.org/10.1093/gji/ggz092.

Ligorria, J.P., and Ammon, C.J., 1999. Iterative Deconvolution and Receiver Function Estimation, *Bulletin of the Seismological Society of America*, 89, 1395-1400, doi.org/10.1785/BSSA0890051395.

Lu, C., Grand, S.P., Lai, H., Garnero, E.J., (2019). TX2019slab: A new P and S tomography model incorporating subducting slabs. *J. Geophys. Res.*, *124*, 11549-11567, doi.org/10.1029/2019JB017448.

Oldenburg, D.W., (1981). A comprehensive solution to the linear deconvolution problem. *Geophysical Journal International*, 65, 331-357, doi.org/10.1111/j.1365-246X.1981.tb02716.x.

Schimmel, M., and Paulssen, H., (1997). Noise reduction and detection of weak, coherent signals through phase-weighted stacks, *Geophysical Journal International*, 130, 497-505, doi.org/10.1111/j.1365-246X.1997.tb05664.x.

Shearer, P.M., (2009). *Introduction to Seismology* (2nd Edition), Cambridge University Press, pp. 102-109 and 245-249.

Thomas C., Kendall J-M., and Weber, M., (2002) The lowermost mantle beneath northern Asia I. Multi-azimuth studies of a D″ heterogeneity. *Geophysical Journal International* 151, 279–295, doi.org/10.1046/j.1365-246X.2002.01759.x

Wysession, M., Wiens, D., Nyblade, A. (2011). Investigation of sources of intraplate volcanism using Passcal broadband instruments in Madagascar, The Comores and Mozambique, [Data set]. International Federation of Digital Seismograph Networks. https://doi.org/10.7914/SN/XV_2011

## Tables

**Table S1:** Stations for source arrays used for this study. Latitude and longitude for stations 1-6 are from the GEOSCOPE website (geoscope.ipgp.fr). Stations 7-9 are stations from other networks. Network and doi are also provided.

| | **station** | **lat** | **lon** | **network** | **doi:** |
|---|---|---|---|---|---|
| 1 | DRV | -66.664908 | 140.002069 | G | doi.org/10.18715/GEOSCOPE.G |
| 2 | AIS | -37.79635 | 77.569186 | | |
| 3 | CRZF | -46.43096 | 51.855308 | | |
| 4 | FOMA | -24.97565 | 46.978877 | | |
| 5 | PAF | -49.351 | 70.210708 | | |
| 6 | RER | -21.1712 | 55.73986 | | |
| 7 | MSEY | -4.6737 | 55.4792 | II | doi.org/10.7914/SN/II |
| 8 | CASY | -66.2792 | 110.5354 | IU | doi.org/10.7914/SN/IU |
| 9 | MAW | -67.604 | 62.871 | AU | dx.doi.org/10.26186/144675 |

**Table S2:** Events used in this study for stations in the Indian Ocean – IO (AIS, CRZF, FOMA, RER, PAF) and MSEY, and stations in Antarctica (DRV, MAW, CASY). Event names indicate the date of the event, OT is the origin time.

| Name | OT | Latitude | Longitude | Depth [km] | Stations |
|---|---|---|---|---|---|
| 1991APR19 | 21:48:35 | -6.900 | 129.562 | 127 | DRV |
| 1991AUG24 | 11:13:19 | -6.065 | 130.368 | 148 | DRV |
| 1991OCT15 | 16:18:01 | -6.494 | 130.043 | 136 | DRV |
| 1991NOV07 | 09:21:23 | -7.320 | 128.550 | 140 | DRV |
| 1992MAY04 | 08:45:01 | -6.762 | 130.229 | 86 | DRV |
| 1992OCT18 | 13:08:54 | -6.279 | 130.214 | 118 | DRV |
| 1992DEC18 | 03:00:44 | -6.541 | 130.417 | 101 | DRV |
| 1993AUG29 | 09:57:54 | -7.005 | 129.560 | 146 | DRV |
| 1994JUN16 | 10:12:46 | -7.391 | 128.125 | 108 | DRV |
| 1994JUL02 | 09:14:43 | -5.763 | 131.103 | 87 | DRV |
| 1994JUL13 | 11:45:23 | -7.532 | 127.77 | 159 | IO |
| 1996FEB28 | 09:44:10 | 1.7560 | 126.048 | 115 | MSEY |
| 1996OCT17 | 16:15:25 | 5.704 | 125.945 | 117 | CASY, DRV |
| 1995DEC25 | 04:43:24 | -6.903 | 129.151 | 141 | DRV, IO |
| 1997DEC22 | 02:05:50 | -5.495 | 147.867 | 179 | IO |
| 1998SEP21 | 06:52:41 | 0.262 | 122.467 | 147 | CASY |
| 1999APR05 | 11:08:04 | -5.591 | 149.568 | -150 | IO |
| 1999DEC13 | 09:30:39 | 2.0770 | 127.1150 | 85 | MSEY |
| 2000MAR03 | 22:09:13 | -7.321 | 128.491 | 141 | DRV, IO |
| 2000JUN14 | 17:00:48 | 4.542 | 127.722 | 90 | DRV |
| 2000SEP26 | 16:49:33 | 1.123 | 127.44 | 142 | CASY |
| 2001SEP18 | 02:19:30 | -7.506 | 127.739 | 131 | DRV, CASY |
| 2001DEC07 | 19:11:31 | -5.645 | 130.742 | 111 | DRV |
| 2001DEC09 | 18:15:02 | -0.002 | 122.87 | 156 | CASY |
| 2002JAN01 | 11:29:22 | 6.303 | 125.650 | 138 | IO, MSEY, DRV |
| 2002MAR19 | 22:14:14 | -6.486 | 129.901 | 148 | DRV |
| 2003MAR10 | 02:09:37 | 1.692 | 127.296 | 93 | IO, MSEY |
| 2004APR17 | 15:58:24 | -7.352 | 128.373 | 128 | DRV |
| 2004JUN30 | 23:37:25 | 0.797 | 124.726 | 90 | IO |
| 2004OCT13 | 20:35:41 | -6.066 | 130.528 | 89 | DRV, CASY, MAW |
| 2007JAN17 | 04:28:26 | -3.322 | 139.834 | 100 | IO |
| 2007JUL01 | 14:34:12 | -5.929 | 130.564 | 134 | DRV |
| 2007DEC15 | 08:03:15 | -7.526 | 127.474 | 175 | CASY, MAW |
| 2008MAR06 | 01:21:59 | 2.572 | 128.232 | 125 | MSEY |
| 2008MAY23 | 22:50:37 | -7.061 | 129.483 | 125 | DRV |
| 2008JUN06 | 13:42:48 | -7.495 | 127.885 | 122 | DRV, IO, CASY, MAW |

| | | | | | |
|---|---|---|---|---|---|
| 2008AUG04 | 20:45:13 | -5.916 | 130.19 | 173 | CASY, MAW |
| 2008SEP11 | 00:00:02 | 1.885 | 127.363 | 96 | IO, CASY |
| 2008OCT20 | 04:54:19 | 0.109 | 120.681 | 96 | CASY |
| 2008OCT21 | 13:00:48 | -7.47 | 127.732 | 135 | DRV, CASY |
| 2008OCT23 | 09:21:15 | 5.957 | 125.778 | 130 | CASY |
| 2008DEC11 | 21:40:51 | 0.063 | 123.433 | 129 | CASY |
| 2009JAN22 | 20:16:34 | -7.307 | 128.56 | 146 | CASY, MAW |
| 2009OCT24 | 14:40:43 | -6.133 | 130.385 | 130 | DRV, IO, MAW |
| 2009SEP18 | 18:34:22 | 1.755 | 127.189 | 93 | CASY |
| 2009DEC26 | 08:57:27 | -5.530 | 131.205 | 85 | DRV, MAW |
| 2010FEB15 | 21:51:47 | -7.217 | 128.723 | 126 | IO |
| 2010MAR26 | 10:39:02 | -6.326 | 130.284 | 124 | DRV |
| 2010AUG15 | 15:09:29 | -5.692 | 148.342 | 174 | IO |
| 2010DEC15 | 11:29:30 | -7.268 | 128.786 | 135 | DRV, IO, MAW |
| 2011JUL12 | 21:06:13 | -6.055 | 130.492 | 131 | DRV |
| 2011DEC13 | 07:52:11 | 0.041 | 123.030 | 161 | IO |
| 2011DEC14 | 05:04:58 | -7.551 | 146.809 | 135 | IO |
| 2012MAR21 | 22:15:06 | -6.242 | 145.955 | 118 | IO |
| 2012APR17 | 07:13:49 | -5.462 | 147.117 | 198 | IO |
| 2012AUG26 | 15:05:37 | 2.190 | 126.837 | 91 | IO |
| 2012DEC10 | 16:53:08 | -6.533 | 129.825 | 155 | IO |
| 2013AUG12 | 00:53:43 | -7.135 | 129.809 | 95 | IO, MAW |
| 2013SEP01 | 11:52:29 | -7.440 | 128.221 | 112 | IO, CASY, MAW |
| 2014DEC06 | 22:05:10 | -6.11 | 130.483 | 116 | IO, CASY |
| 2015JUN15 | 21:04:24 | 4.1537 | 125.8447 | 136 | CASY |
| 2015NOV21 | 09:06:13 | -7.148 | 129.937 | 82 | DRV, CASY |
| 2015DEC24 | 23:10:58 | -7.218 | 128.977 | 119 | DRV, MAW |
| 2016OCT09 | 14:46:26 | 1.7703 | 127.449 | 128 | CASY |
| 2016DEC04 | 05:24:05 | 4.5051 | 127.8342 | 139 | DRV |
| 2016DEC21 | 00:17:14 | -7.508 | 127.921 | 152 | IO, CASY |
| 2017JUL15 | 12:12:21 | 0.4098 | 121.9844 | 113 | CASY |
| 2017NOV07 | 21:26:38 | -4.243 | 143.485 | 110 | IO |
| 2017DEC15 | 16:47:58 | -7.492 | 108.174 | 90 | IO |
| 2018MAR25 | 08:58:10 | -6.634 | 129.817 | 169 | DRV, IO, MAW |
| 2018DEC01 | 13:27:21 | -7.384 | 128.707 | 136 | DRV, IO, CASY |
| 2019MAY06 | 21:19:37 | -6.975 | 146.449 | 146 | IO |
| 2019MAY31 | 10:12:32 | 6.2795 | 126.479 | 99 | CASY, MSEY, DRV |
| 2019JUN14 | 20:10:52 | -5.843 | 130.725 | 105 | DRV, MAW |
| 2020MAY06 | 13:53:55 | -6.776 | 129.785 | 96 | DRV, IO, CASY, MAW |
| 2020JUN04 | 08:49:40 | 2.911 | 128.248 | 112 | MSEY |
| 2020SEP06 | 15:23:43 | 6.2693 | 125.8285 | 120 | CASY, DRV |

| | | | | | |
|---|---|---|---|---|---|
| 2020SEP08 | 00:45:20 | -4.8713 | 129.7548 | 172 | MAW |
| 2020NOV01 | 03:43:20 | -7.071 | 129.2407 | 182 | MAW |
| 2021JAN06 | 20:59:34 | 0.0658 | 122.9487 | 148 | CASY |
| 2021DEC04 | 23:47:55 | 4.0932 | 128.1359 | 149 | DRV |
| 2021DEC29 | 18:25:51 | -7.548 | 127.577 | 165 | IO, CASY |
| 2022FEB01 | 19:25:10 | -7.483 | 128.313 | 119 | DRV, CASY |
| 2022AUG09 | 12:59:40 | -6.723 | 129.954 | 149 | DRV |
| 2023JAN18 | 00:34:45 | -0.0116 | 123.1998 | 154 | CASY |
| 2023FEB23 | 20:02:47 | 3.2796 | 128.1356 | 92 | MSEY |
| 2023MAY24 | 15:49:34 | -6.9484 | 129.5293 | 158 | CASY, MAW |
| 2023SEP11 | 12:51:33 | 1.1246 | 127.4888 | 151 | CASY |
| 2023SEP26 | 01:39:43 | 4.7109 | 127.5053 | 94 | CASY, DRV |
| 2023OCT04 | 11:21:47 | 5.3171 | 126.0438 | 113 | MSEY, DRV |
| 2023NOV22 | 02:48:5 | 1.7827 | 127.1887 | 102 | CASY |
| 2024SEP23 | 19:51:02 | -0.0469 | 122.8918 | 143 | CASY |

**Table S3:** Events used for receiver array verification (e.g., Figure S6, Figure 9 and S8). The arrays are in Madagascar (Wysession et al., 2011), Tanzania (Ebinger 2013) and the Beetaloo Seismic Monitoring Project (BTL) in Australia.

| Name | OT | Latitude | Longitude | Depth [km] | Array |
|---|---|---|---|---|---|
| 2012Aug26 | 15:05:37 | 2.19 | 126.84 | 91 | Madagascar, XV doi.org: 10.7914/SN/XV_2011 |
| 2014Jan25 | 05:14:18 | -7,98 | 109.26 | 66 | Tanzania, XJ doi.org: 10.7914/SN/XJ_2013 |
| 2021Oct02 | 20:43:39 | -9.178 | 67.261 | 10 | Australia (BTL), 2O doi.org/10.7914/SN/2O_2019 |
| 2022Mar27 | 00:50:45 | -13.807 | 66.176 | 13 | |

**Figure S1:** Source array traces (Z-components) for stations FOMA, DRV, AIS and PAF. Theoretical P and PcP arrivals are indicated for the centre station. Note that for AIS, despite good signal quality, only four traces are available in the cluster around 70 degrees epicentral distance and six traces between 55 and 60 degrees. The epicentral distance of FOMA is between 77.5 and 82 degrees, with P and PcP starting to merge at these large distances.

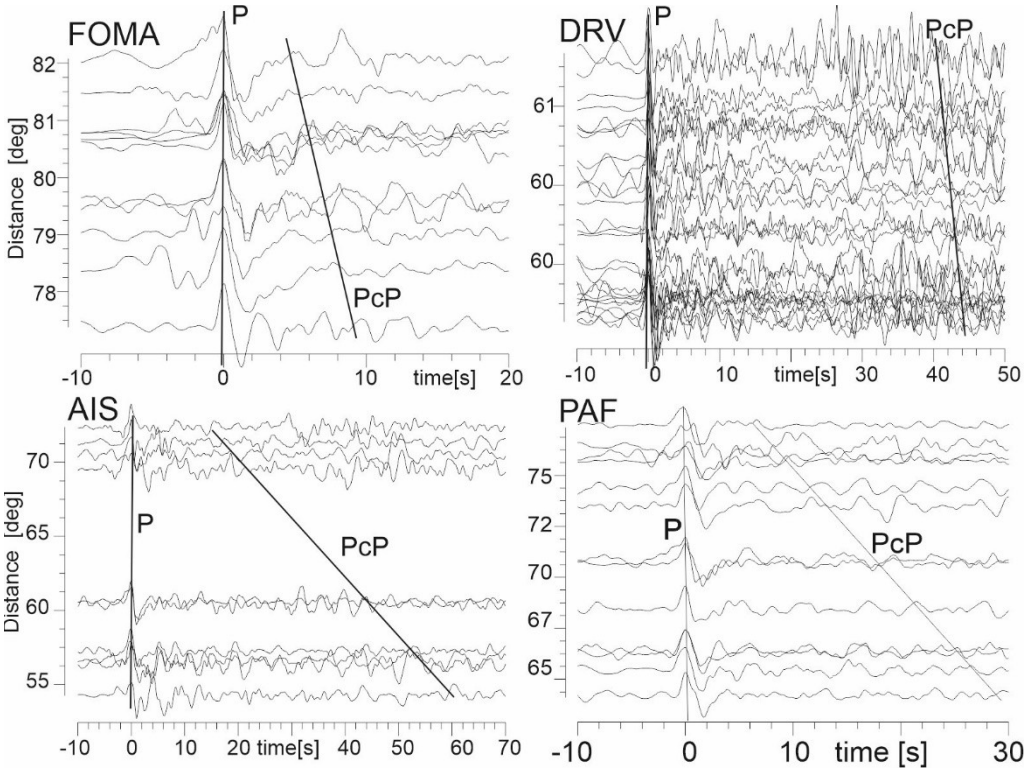

**Figure S2:** Traces for station PAF: a) raw traces (unfiltered, no source normalisation). Note that we already tried to pick events with similar source wavelets. All deconvolution methods in the following panels are applied to traces filtered with a second order butterworth bandpass filter of 2-12 s. b) traces without source normalisation, i.e., only filtered, c) spiking deconvolution (SD) d) Hilbert Transform (HIL) and e) cross-correlation (CORR).

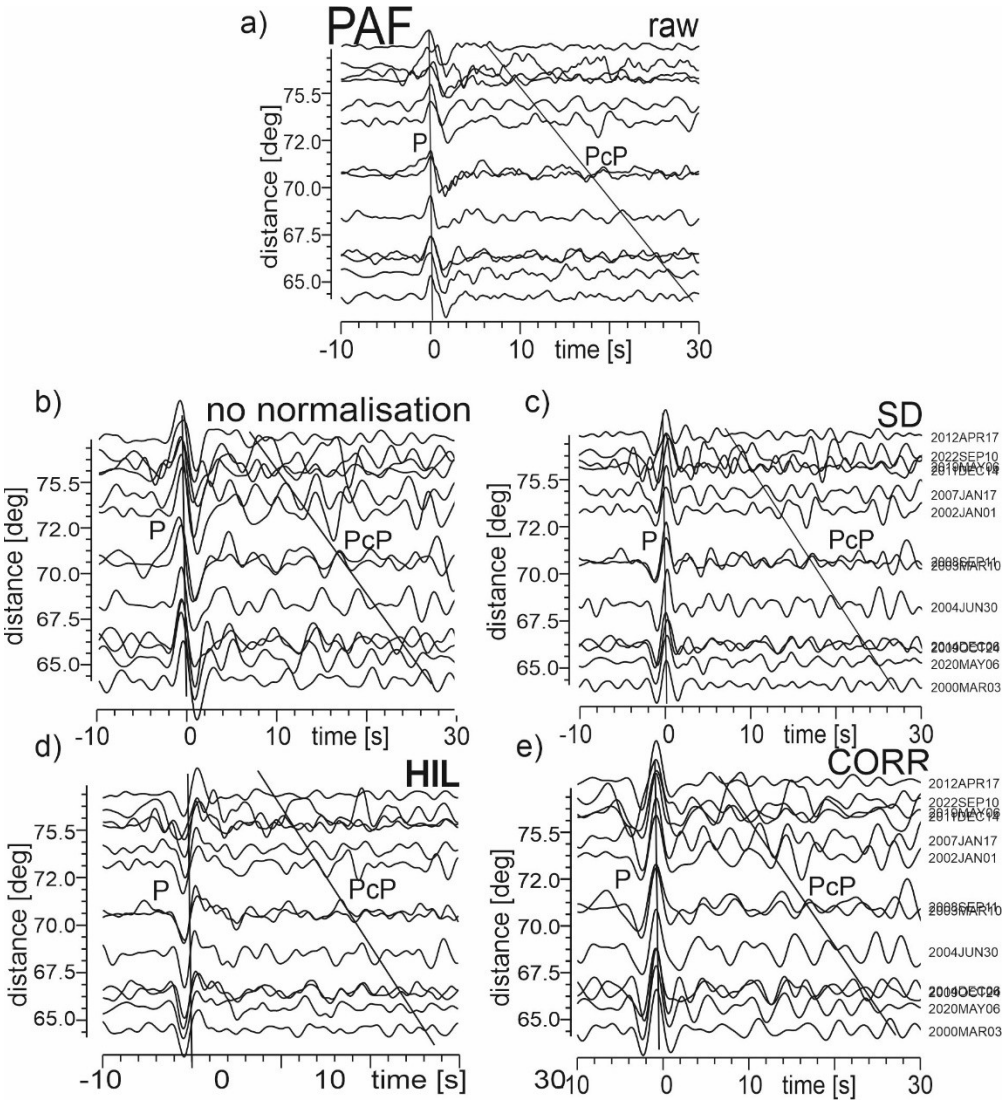

**Figure S3:** Source vespagram test for station CRZF with initial alignment of traces on the P-wave (a) and the PcP wave (b) before stacking. The aligned wave is used for reference and in the source-vespagram set to the theoretical backazimuth and slowness. Since the differential travel times of the P, PdP and PcP wave differ for each event, the stack enhances only the wave for which the traces were aligned. Other waves will not stack coherently because the wave arrival times differ from the calculated arrival times. This may lead to a variation in slowness or even a diminishing of the wave amplitude or waveform.

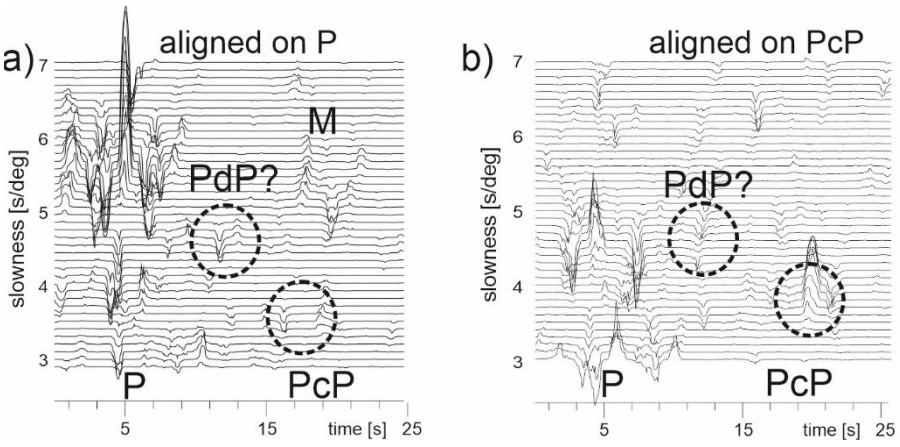

**Figure S4:** Principle of our migration images and amplitude depth profiles. At each depth: For each grid point the traces are shifted and stacked with the calculated delay times for each source and receiver combination, and the stacked amplitude is assigned to the respective grid point on a latitude-longitude grid (See also Figure 5 and explanation in the main text). Energy will spread out along an isochrone (i.e., the elliptical red ring). If there is a two-sided wavelet, a second ellipse with high amplitudes (here in blue) will follow around the red ellipse. As the depth increases, the region of large amplitudes will arrive at shorter times, i.e., the size of ellipse(s) of large amplitudes will decrease. The point where the large red amplitude focusses (Depth 4) is the point, where we pick the reflection. Ideally, the focussing point lies in the theoretical reflection point. At later times (i.e., deeper depth), the blue ellipse will focus. The amplitude-depth profile shows the stacked amplitude for the theoretical reflection point of the source-receiver combination for the central earthquake (or for the central station in case of a receiver array).

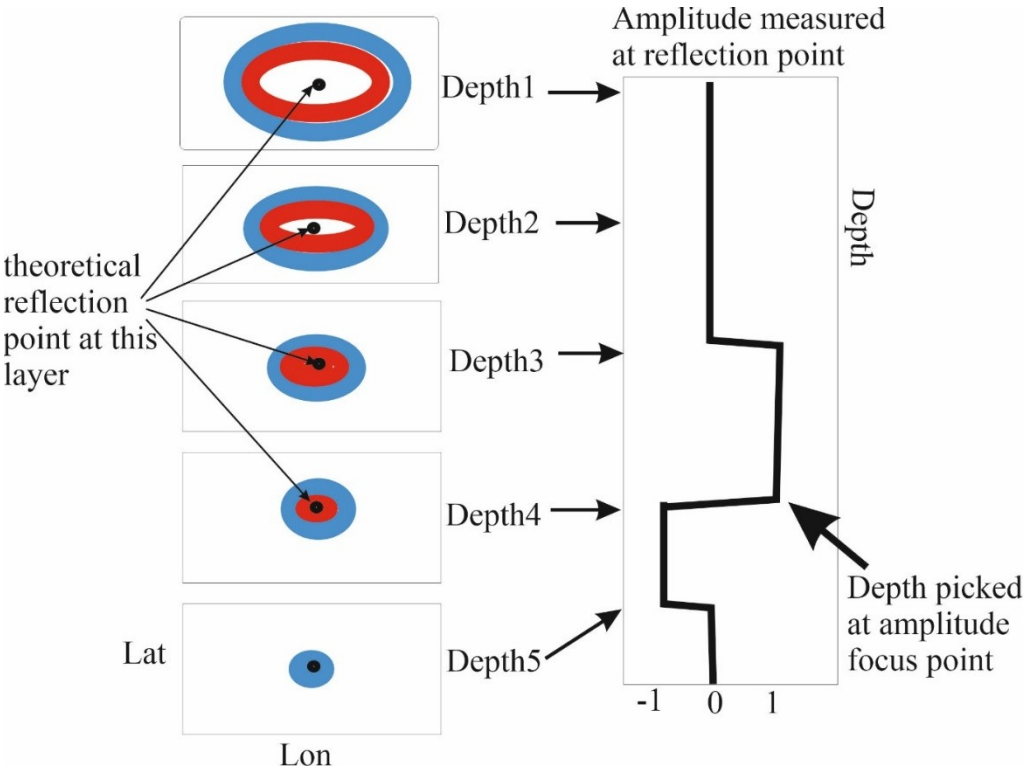

**Figure S5:** Amplitude-depth profiles and migration images for the relevant depth of PdP and PcP for stations CRZF (a) and PAF (b), indicated by the dashed lines in the amplitude depth profiles. Note that for station PAF the images are less clear. Filters used for the stations are given in brackets following station names. The stacked amplitudes of PdP and PcP for CRZF in the amplitude-depth profile are small and focussing off-centre in the scatter plot for 2630km and 2900km depth. The results are therefore marked as less reliable than results for RER and stations in Antarctica.

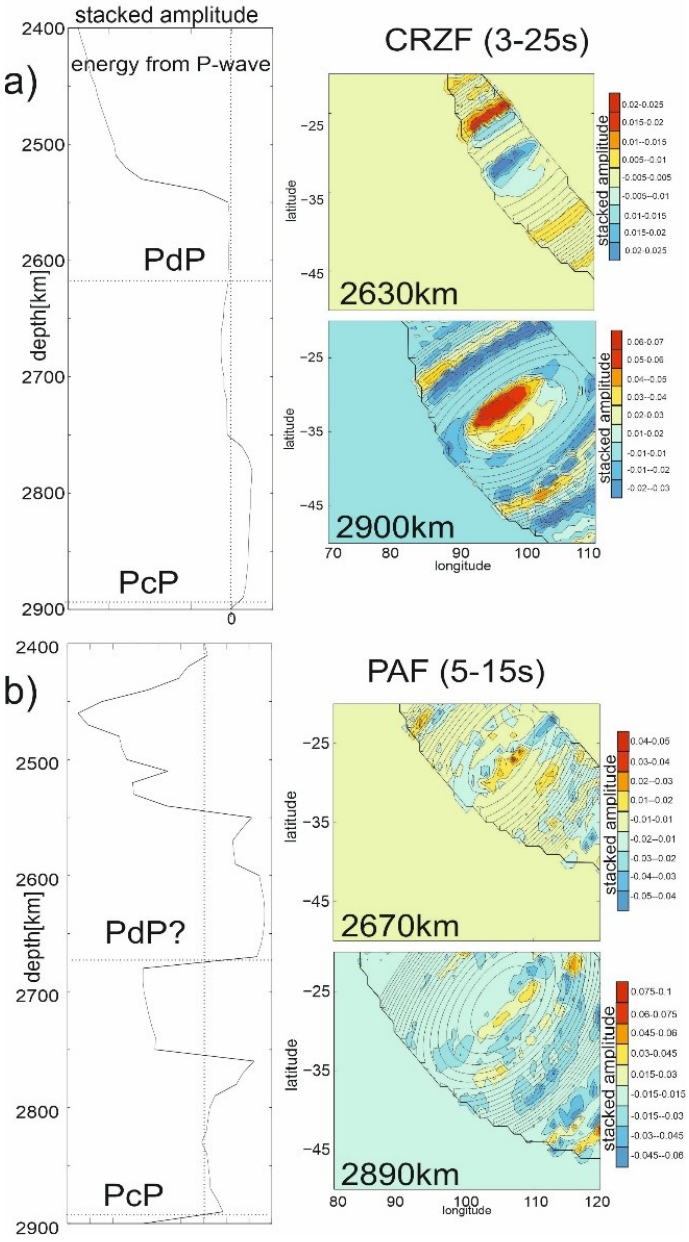

**Figure S6: a)** Amplitude-depth profile for CASY with events in the northern cluster (Fig 2) – labelled as CASY2. **b)** Additional examples of amplitude depth profiles from the source migration of stations MAW, MSEY and CASY (southern cluster, labelled as CASY1).

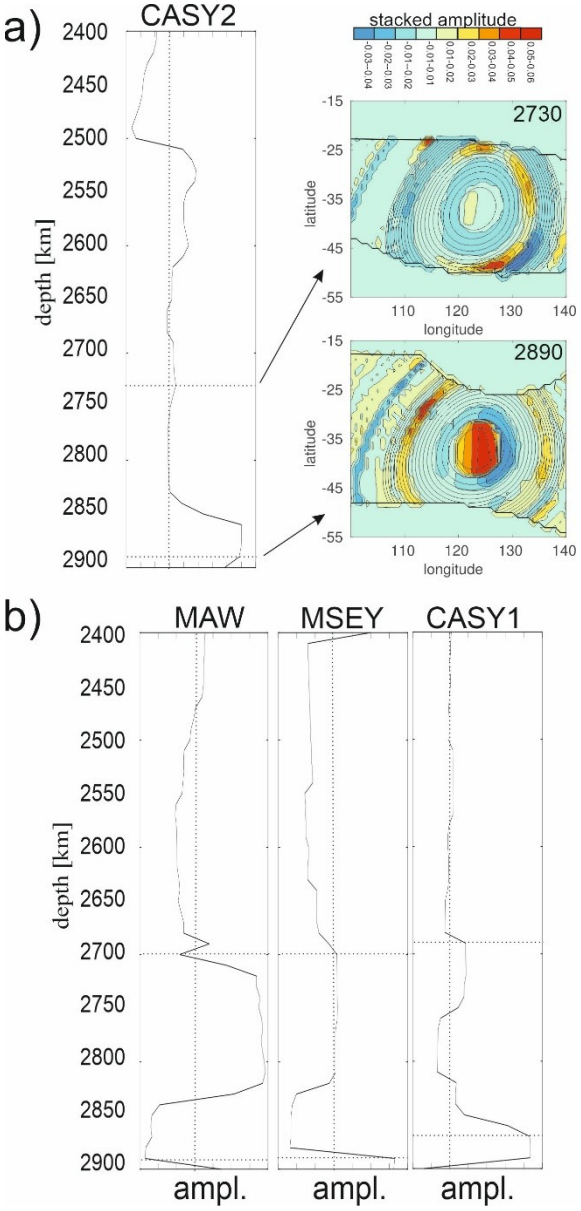

**Figure S7:** Amplitude-depth profile from the migration using synthetic data for PAF (similar to Figure 6 in the main text) but generated with AxiSEM3D (Leng et al., 2019) and TX2019slab (Lu et al., 2019) as 3D input model. The synthetics were generated for a minimum period of 5s, i.e., longer than those shown in Figure 6. The dashed line is amplitude 0. This test shows that finite frequency effects cannot generate the reflections we find in the real data. The amplitude depth profile does not cross the zero line before PcP.

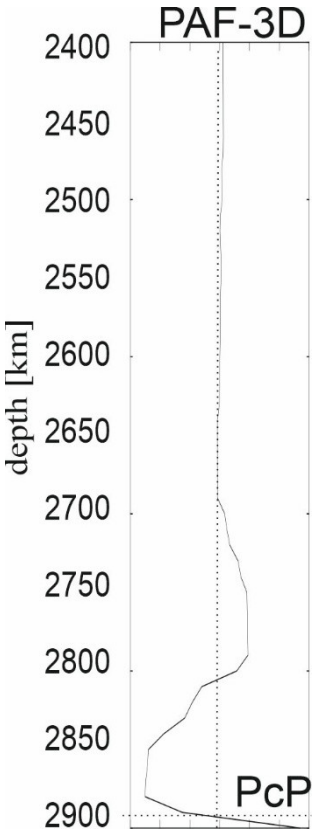

**Figure S8:** Receiver-array traces (a, b) using stations in Ethiopia (left) and Madagascar (right) and the corresponding vespagrams (c-f) for P-waves (middle panel) and S-waves (bottom panel). The data in a) and c) are filtered with a bandpass filter from 0.3 to 3s, b) and d) bandpass 1 to 10s, e) bandpass 2 to 12 s and f) bandpass 3 to 25 s. The arrivals of P, PdP, S, SdS, PcP and ScS are marked by the red ellipses. The reflection point for these events are in the southern part of the area imaged by YL87 shown in Figure 9 in the main text.

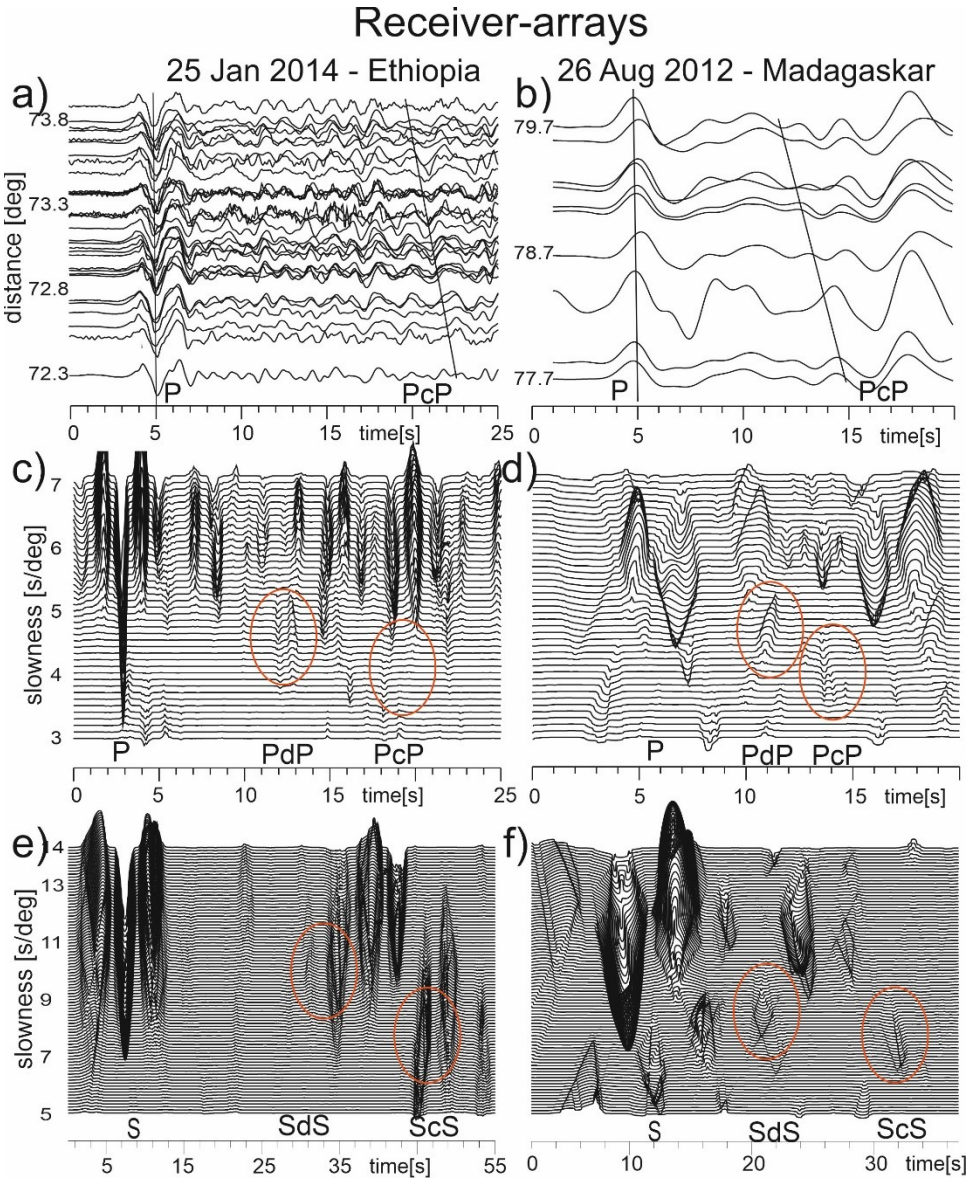

**Figure S9:** As Figure 9, but with the vote map for the Indian Ocean for lower than average P-wave velocities at depth 2600 km.